scientific reports

Check for updates

OPEN

SLC11A1 can activate TGF-β1 signaling pathway to resist ferroptosis in colorectal cancer

DongQiang Yang[1], LianMei Zhao[2], Ping Shi[3], Jianfeng Zhang[4], Guang Yang[1], Bo Shi[1], Hongqing Ma[4], Baokun Li[4], Feifei Wang[4] & Guiying Wang[4,5,6]✉

High expression of Solute Carrier Family 11 Member 1(SLC11A1) leads to a poor prognosis in patients with CRC, while the specific role of SLC11A1 in CRC remains unreported. Therefore, this study mainly addressed the preliminary mechanism and specific role of SLC11A1 in CRC. The results showed that six subsequent genes were successfully screened by the line database, and the abnormal expression of SLC11A1 was the most obvious in colorectal cancer patients. Following phenotypic experiments demonstrated that SLC11A1 promoted proliferation, invasion and migration of colorectal cancer cells. SLC11A1 Is also able to downregulate Acyl-CoA Synthetase Long Chain Family Member 4 (ACSL 4), Cyclooxygenase-2 (COX2), NADPH Oxidase 1 (NOX1) and upregulate the expression levels of Hypoxia-Inducible Factor 1 (FIH1), Glutathione Peroxidase 1 (GPX1) protein, inhibit the expression levels of MDA and Fe^{2+} in colorectal cancer cells, and resist ferroptosis in colorectal cancer cells. SLC11A1 Overexpression can up-regulate the protein expression level of TGFβ1 (Transforming Growth Factor Beta 1), p-Smad 2 / 3, activate TGFβ1 signaling pathway activity, and promote colorectal cancer cell progression. In conclusion, we successfully demonstrated that SLC11A1 confers resistance to ferroptosis in colorectal cancer cells, providing a potential target for the clinical treatment of colorectal cancer.

Keywords Colorectal cancer, Solute carrier family 11 member 1, Transforming growth factor beta 1 signaling pathway, Ferroptosis, Invasion and metastasis

Abbreviations

CRC	Colorectal cancer
SLC11A1	Solute carrier family 11 member 1
ACSL4	Acyl-CoA synthetase long chain family member 4
COX2	Cytochrome c oxidase subunit II
FIH1	Factor inhibiting hypoxia-inducible factor 1 alpha
GPX4	Glutathione peroxidase 4
NOX1	NADPH oxidase 1
Smad2/3	Family Member2/3
TGFβ1	Transforming growth factor beta 1

Colorectal cancer (CRC) is the third commonly diagnosed cancer and the second cause of cancer death worldwide[1]. 20% of newly diagnosed CRC patients have distant metastases at presentation, and another 25% of CRC patients will have metastases during the course of their disease[2]. Approximately 90% of stage IV patients present with liver, lung, brain, or peritoneal metastases[3]. Metastatic colorectal cancer remains a deadly disease, with a 5-year survival rate of about 14%[4]. Currently, targeted therapies for CRC include surgery, immunotherapy, targeted therapy, and chemotherapy[5]. With the progress of treatment methods, the mortality rate of colorectal

[1]Department of Radiology, The Fourth Hospital of Hebei Medical University, Shijiazhuang 050000, Hebei, China. [2]Scientific Research Center, The Fourth Hospital of Hebei Medical University, Shijiazhuang 050000, Hebei, China. [3]Otorhinolaryngology Head and Neck Surgery, The Fourth Hospital of Hebei Medical University, Shijiazhuang 050000, Hebei, China. [4]The Second Department of General Surgery, The Fourth Hospital of Hebei Medical University, Shijiazhuang 050000, Hebei, China. [5]Department of General Surgery, The Second Hospital of Hebei Medical University, Shijiazhuang 050000, Hebei, China. [6]Hebei Key Laboratory of Etiology Tracing and Individualized Diagnosis and Treatment for Digestive System Carcinoma, The Second Hospital of Hebei Medical University, Shijiazhuang 050000, Hebei, China. ✉email: wangguiying@hebmu.edu.cn

cancer patients has decreased in developed countries[6], but the early screening and late treatment of colorectal cancer are particularly important, and the development of new targeted drugs is urgently needed.

The regulatory mechanism of TGFβ signaling pathway is very complex, involving the interaction of multiple molecules and signaling pathways[7]. For example, TGFβ signaling pathway can be regulated by other signaling pathways, such as MAPK signaling pathway, PI3K/Akt signaling pathway, and Wnt/β-catenin signaling pathway[8]. In addition, the TGFβ signaling pathway can also be regulated by a variety of intracellular and extracellular factors, such as cytokines, growth factors, hypoxia and oxidative stress[9]. A large number of studies have shown that TGFβ signaling pathway plays an important role in the occurrence, development and metastasis of colorectal cancer[10]. For example, TGFβ signaling can promote the proliferation, migration, and invasion of colorectal cancer cells, and inhibit apoptosis[11]. In addition, TGFβ signaling can also promote angiogenesis and immune escape, thereby promoting the growth and metastasis of colorectal cancer. Inhibition of TGFβ signaling pathway is a new way to treat colorectal cancer[12–14].

In this study, we performed a systematic bioinformatics analysis using single-cell RNA sequencing (scRNA-seq) and bulk RNA-seq data to identify monocyte / neutrophil marker genes and construct a diagnostic signature to verify its diagnostic value through an external validation cohort. In addition, we also selected a genetic diagnostic feature for further functional exploration. Overall, our study may help to identify a novel metastasis-specific biomarker for colorectal cancer.

Materials and methods

Dataset acquisition and processing

ScRNA-seq data from 6 primary CRC samples of GSE188711 were obtained from the GEO database and used to determine the monocyte/neutrophil marker genes of CRC. In addition, transcriptome expression profiles of GSE81558, GSE41258 and GSE81581 were downloaded as well. GSE81558, included 23 tumor tissues and 19 paired liver metastases, was served as training set, GSE41258, included 186 tumor tissues and 47 paired liver metastases, was served as validation set, and GSE81581 (miRNA dataset), included 23 tumor tissues and 19 paired liver metastases, was used to construct the ceRNA network.

Identification of monocyte/neutrophil marker genes by scRNA-seq analysis

ScRNA-seq data of GSE188711 was analyzed using the "Seurat" and "SingleR" packages in R software. A total of 33,482 cells from 6 primary CRC samples were included in this analysis. Quality control for the scRNA-seq data was performed by removing genes expressing less than 3 single cells, cells with less than 200 mapped genes and cells with more than 5% of mitochondrial genes. Gene expression of remaining cells was normalized using a linear regression model, and then the top 1500 genes with highly variable characteristics were screened by ANOVA. Principal component analysis (PCA) was performed on single-cell samples, and the top 20 principal components (PC) were selected for subsequent analysis. T-distributed stochastic neighbor embedding (t-SNE) was used for dimensional reduction and unsupervised clustering. The limma packages in R software was used to compare the differences of gene expression between a cluster and all other clusters. To identify the marker genes for each cluster, $|\log_2 (\text{fold change})| > 1$ and adjusted $p < 0.05$ were used. Finally, the "SingleR" package was used to annotate the cell subpopulations of the different clusters.

Identification of hub genes

With limma package, the differentially expressed genes (DEGs) between CRC and CRLM in GSE81558 were obtained ($p < 0.05$). Heatmaps and volcano plots of DEGs were visualized using pheatmap and ggplot packages in R, respectively. The hub genes were acquired by overlapping monocyte and neutrophil marker genes with DEGs, respectively. Functional enrichment analysis for these hub genes were conducted with DAVID database ($p < 0.05$). PPI network was constructed for these hub genes with STRING database.

Tumor immune microenvironment (TIME) analysis

With single sample gene set enrichment analysis (ssGSEA), the relative abundance of immune cell in TIME of CRC and CRLM were quantified. Enrichment scores calculated by ssGSEA analysis were used to represent the relative abundance of immune cell in TIME of patients to observe differences between monocytes and neutrophils in CRC and CRLM. In addition, the correlation between hub genes and monocyte/neutrophil was analyzed by the Pearson correlation coefficient.

Construction and validation of a diagnostic signature

To minimize overfitting, least absolute shrinkage and selection operator (LASSO) logistic regression algorithm was employed to select feature genes and construct diagnostic signature for CRLM via using "glmnet" package. Then, receiver operating characteristic (ROC) curves were used to assess the prediction ability of the signature using pROC package. The predictive ability of the signature was validated in validation set as well.

Construction of CeRNA network and TF regulatory network

Based on ENCORI database, the miRNA-mRNA and miRNA-lncRNA interaction pairs for the feature genes were predicted. The differentially expressed miRNAs between CRC and CRLM were obtained in GSE81581 ($p < 0.05$). The correlation analysis between lncRNAs and feature genes were performed ($p < 0.05$). For the purpose of obtaining more reliable prediction results, only the miRNA differentially expressed in GSE81581 and lncRNAs associated with feature genes were selected to construct the ceRNA network. A transcription factor (TF) subset was obtained from Cistrome, and corresponding TF expression values were obtained from the training set. With correlation analysis, TFs associated with the feature genes ($|r| > 0.5$, $p < 0.05$) were selected for the construction of TF regulatory network.

Cell lines and cell culture

The human CRC cell lines (CACO2, HCT116, HT29, LOVO, SW480, SW620) and normal colorectal mucosa cell line (NCM460) were used in this study. These cell lines were cultured in medium containing 10% of fetal bovine serum, 1% of double antibiotics and 5% of CO_2 at 37 °C. The cell lines used in this study were purchased from Wuhan Prosai Life Technology Co., Ltd (China). All methods were performed in accordance with the relevant guidelines and regulations.

RT-qPCR in human subjects and cell lines

Formalin-fixed, paraffin-embedded (FFPE) specimens of 5 colorectal adenocarcinomas and 5 paired liver metastases were obtained from 5 patients with CRLM after informed consent had been given by each subject. Total RNA from FFPE specimens was extracted from recently cut 5–10 μm FFPE sections using the RNAprep pure FFPE Kit (TIANGEN, Beijing, China) according to the manufacturer's protocol, using 2–8 sections per case depending on assay. Total RNA was isolated from cells in cell lines (NCM460, SW480 and SW620) with TRIzol reagent (Thermo Fisher Scientific, Inc., Waltham, MA, USA). RT-qPCR was performed in an ABI StepOne Plus System with SuperReal PreMix Plus (SYBR Green) (TIANGEN, Beijing, China). The reaction was set at 95 °C for 15 min for pre-denaturation, then at 95 °C for 10 s, at 55 °C for 30 s, and 72 °C for 32 s repeating 40 cycles. Relative gene expression was analyzed by $2^{-\Delta\Delta CT}$ method[15]. GAPDH and ACTB were used as endogenous controls. The primers of RT-qPCR were listed in Table S1.

Cell transfection

For transfection of siRNA and overexpression plasmid, siRNA and overexpression plasmid targeting human SLC11A1 were synthesized from HippoBio (Huzhou, China) (see Table S2 for sequence information). One 106 cells was plated in a 6-well plate and cultured in 37 C. When the cell concentration reached 50%, the specific siRNA and the overexpression plasmid were transfected with Lipo8000TM (Shanghai Biyuntian Biological Co., Ltd Biotech, Shanghai, China). Forty-eight hours after transfection, the mRNA and protein expression of SLC11A1 were determined by RT-qPCR and Wesetern blot.

Experimental groups

To further explore the targeted regulatory effect of SLC11A1 on the TGFβ1 signaling pathway, three experimental conditions were set in HCT116 cells: the Vector group, the oe-SLC11A1 group, and the LSKL (an inhibitor of the TGFβ1 pathway) combined with oe-SLC11A1 group. In the LSKL combined treatment group, 5 μmol/L LSKL (HY-P7118, MedChemExpress, China) was added 48 h after transfection, and the cells were cultured for an additional 24 hours[16].

In HT29 cells, the experiments were divided into the si - NC group, the si - SLC11A1–1 group, and the si-SLC11A1-1 combined with TGFβ1 (10 ng/mL) group[17]. In the combined treatment group, 10 ng/mL TGFβ1 (HY-P0299, MedChemExpress, China) was added 48 h after transfection, and the cells were cultured for another 24 h to activate the TGFβ1 signaling pathway.

RT-qPCR and WB

Total RNA was isolated from cells with TRIzol reagent according to the manufacturer's procedure. RT-qPCR was performed in an ABI StepOne Plus System with SuperReal PreMix Plus (SYBR Green). Relative gene expression was analyzed by $2^{-\Delta\Delta CT}$ method. The protein was extracted from cells to determine protein concentration, followed by SDS-PAGE gel electrophoresis and then transferred to a polyvinylidene fluoride (PVDF) membrane. The membranes were blocked with 5% BSA at room temperature and incubated with primary and secondary antibodies. Protein detection was achieved with the ECL chemiluminescence kit for further analysis of bands. Primer sequences for RT-qPCR are detailed in Table S1. For detailed information on the antibodies and their dilution ratios used in the Western blot experiments, please refer to Table S2 in the Supplementary Materials.

Cell counting Kit-8 (CCK-8) assays

The cell viability was detected using the CCK-8 assay kit (K2268, APExBIO, USA). HCT116 and HT29 cells in the exponential growth phase were selected for the experiment. After successful transfection, trypsin (CA1210, Beijing Solarbio Science&Technology Co.,Ltd, China) was added to digest the cells. The cells were then centrifuged at 1200 g for 3 min. Subsequently, culture medium was added to make a cell suspension, and the cell density was calculated using a cell counter (Countess, Thermo Fisher Scientific, China). The cells were seeded into 96-well plates at a density of 3×10^3 cells per well and cultured for 24 h, 48 h, and 72 h respectively. Subsequently, 10 μL of CCK-8 solution was added to each well, and the cells were incubated at 37 °C for 4 h. After that, the absorbance was measured at 450 nm.

Transwell assays

Before the experiment, the cells were starved in serum-free medium for 12 h. Cells were treated with trypsin, resuspended in PBS and cell density was adjusted to 2×10^5/ml in serum-free medium containing 0.1% of BSA. 100 μl cell suspensions were seeded into a transwell chamber (BD, USA), which was coated with (invasion) or without (migration) Matrigel (Yeasen, Shanghai, China). After 48 h incubation, the cells were fixed in 4% tissue cell fixation solution for 20 min, and then stained with crystal violet at room temperature for 5 min. Microscope photography was performed.

EDU staining

The exponentially growing colorectal cancer cells were added with EDU solution (Shanghai Biyuntian Biological Co., Ltd, C0075S, China) and incubated at a final concentration of 10 μmol/L for 2 h, and then the cells were

fixed for 30 min by removing the cell medium and adding 4% paraformaldehyde (Shanghai Biyuntian Biological Co., Ltd, P0099, China). The cell culture medium was removed, and the cells were incubated with 0.5%Triton X-100(Shanghai Biyuntian Biological Co., Ltd, P0096, China) for 10 min, and DAPI dye (Shanghai Biyuntian Biological Co., Ltd, C1002, China) for 5 min. After incubation, photos were taken by fluorescence microscope, and the EDU positive cells were statistically analyzed by Image J 1.5.2a.

Cell wound scratch assay

Using a sterile pipette wash, the hair is gently brushed across the exponentially growing colorectal cancer cells, creating a straight scratch. The detached cells were washed with sterile PBS and fresh medium was added. At different points in time, the scratched area is viewed with a microscope and photographs are taken. The photos were statistically analyzed by Image J 1.5.2a software.

Electron microscopy

Cells were digested and centrifuged as described, and treated cells from each group were collected and fixed with glutaraldehyde(Shanghai Mailin Biochemical Technology Co., Ltd, G849973, China) for 30 min, before 4℃ transport to Wuhan Servicebio Technology CO.,LTD (China) for electron microscopy for mitochondrial morphology changes. The next step is simply to remove the excess fixative with a phosphate buffer. Osmium acid was added to the rinsed cells and dehydrated with increasing concentrations of ethanol, after which the cell mitochondrial morphology changes were observed by electron microscopy.

MDA and Fe^{2+} detection

The cell samples were processed according to the requirements of iron content (Elabscience, E-BC-K881-M, China) and MDA (Elabscience, E-BC-K028-M, China) detection kit, and the content of Fe^{2+} and MDA in the cells was detected. The Fe^{2+} content was determined and the OD value (593 nm) was detected using SpectraMax Mini multifunctional enzyme marker. The OD value (532 nm) of MDA content was detected using SpectraMax Mini multifunctional enzyme marker. The formulas for calculating the Fe^{2+} and MDA contents are detailed in the Supplementary Materials.

Co-immunoprecipitation (Co-IP) experiment

HCT116 and HT29 cells were treated according to the description of the cell experimental groups. After the treatment, trypsin solution was added to collect the cell suspension, which was then centrifuged at 1200 g for 3 min. Protein A + G magnetic beads were prepared according to the instructions of the immunoprecipitation kit (P2179, Shanghai Biyuntian Biological Co., Ltd Biotechnology, China). 500 µL of the antibody working solution or 500 µL of the normal IgG working solution was incubated at 25 °C for 1 h, and then washed three times with 500 µL of TBS. 20 µL of the magnetic bead suspension was added to every 500 µL of the protein sample, and the mixture was incubated overnight at 4 °C. After incubation, the sample was placed on a magnetic stand for 10 s for separation. The supernatant was collected into a new centrifuge tube, and the obtained protein sample was subjected to Western blot analysis.

Statistical analysis

All experiments were independently repeated at least three times, and the data are presented as the mean ± standard deviation (SD). All methods were performed in accordance with the relevant guidelines and regulations. Statistical analysis was performed using GraphPad Prism 9.0 software. A two-tailed Student's t - test was used for comparisons between two groups. For comparisons among multiple groups, one-way analysis of variance (ANOVA) was applied, followed by Tukey' s multiple-comparison test for post-hoc analysis. For high-throughput data involving multiple statistical comparisons, the Bonferroni correction was applied to control the false-positive risk resulting from multiple hypothesis testing. The predictive performance of the diagnostic model was evaluated using receiver operating characteristic (ROC) curve analysis, and the area under the curve (AUC) was presented with a 95% confidence interval (CI). The correlation between variables was evaluated by the Pearson correlation coefficient. P-value < 0.05 was considered to indicate a statistically significant difference.

Results

Identification of monocyte/neutrophil marker genes by scRNA-seq analysis

The analysis ideas and procedures for the online database are shown in Fig. S1. According to quality control criteria, low-quality cells and genes were excluded, leaving 11,330 cells for subsequent analysis (Fig. 1A). A total of 22,852 genes were detected in all cells, with 1500 highly variable genes (Fig. 1B). The PCA method was used for dimensionality reduction, and 20 PCs with $p < 0.05$ were selected for further analysis (Fig. 1C). Afterwards, the core cells were classified into 14 independent cell clusters using the t-SNE algorithm (Fig. 1D). Different cell clusters have distinct gene expression profiles, and some genes differentially expressed among the 14 clusters. The "singleR" algorithm was applied to annotate cell subpopulations, clusters 6 and 7 were defined as neutrophil and monocyte subpopulations, respectively (Fig. 1E). Ultimately, 345 neutrophil marker genes and 122 monocyte marker genes were obtained with $|\log_2 FC| > 1$ and adjusted p-value < 0.05.

Identification of hub genes

With $p < 0.05$, 1546 DEGs between CRC and CRLM in GSE81558 were obtained (Fig. 2A-B). By overlapping 122 monocyte and 345 neutrophil marker genes with 1546 DEGs, 37 hub genes were obtained. To elucidate the potential functions of these hub genes, functional enrichment analysis was performed (Fig. S2A-B). GO analysis revealed that the biological processes (BP) mainly involved cytoplasmic translation, aging and inflammatory response. In terms of cellular component (CC), these genes were mainly implicated in cytosol, cytoplasm and

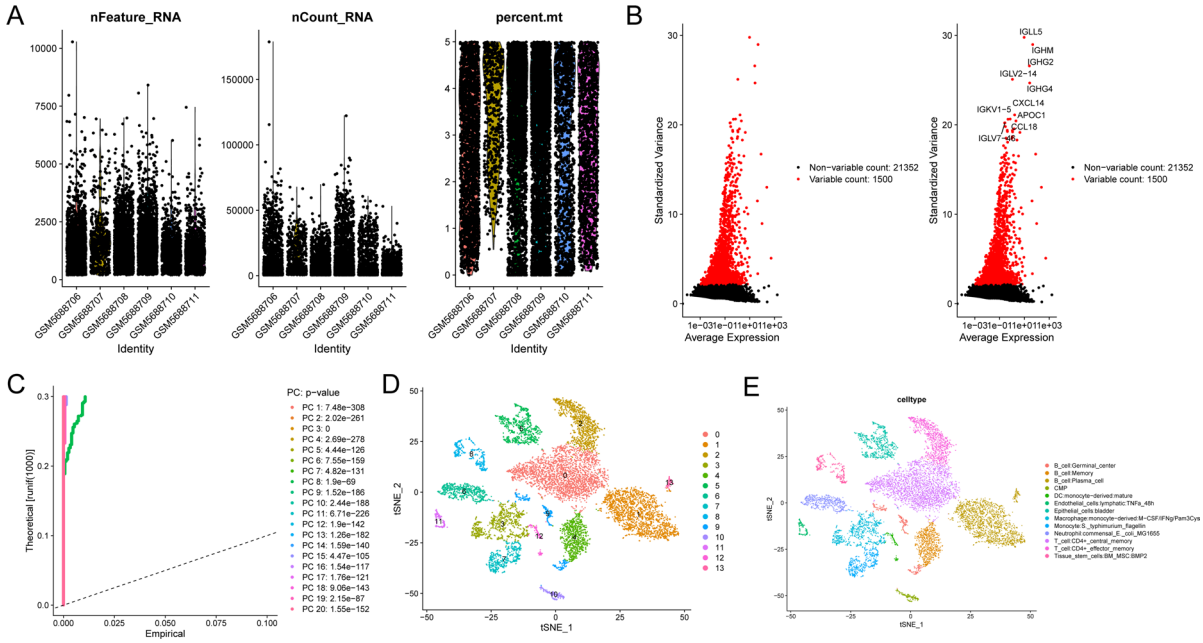

Fig. 1. Identification of monocyte/neutrophil marker genes by scRNA-seq analysis. (**A**) Quality control of scRNA-seq data from 6 CRC samples. (**B**) The variance plot showed 22,852 genes in all cells, red dots represent the top 1500 highly variable genes. (**C**) 20 PCs were identified based on $p < 0.05$. (**D**) 14 clusters were visualized based on the t-SNE algorithm. (**E**) Cell subpopulations identified by marker genes.

nucleus. In molecular function (MF), protein binding, RNA binding and structural constituent of ribosome were the predominant categories. KEGG analysis indicated that these genes were enriched in multiple pathways, such as MAPK signaling pathway, Lipid and atherosclerosis, Toll-like receptor signaling pathway and HIF-1 signaling pathway. In addition, the PPI network of hub genes showed the linkage between each hub gene (Fig. S2C).

Immune cell analysis

The ssGSEA was used to estimate the infiltration levels of monocyte and neutrophil in training and validation set. In the training set, results of the ssGSEA algorithm found that the immune cell infiltration levels of monocyte and neutrophil were significantly higher in the CRLM group (Fig. 2C). In the validation set, monocytes also showed a significantly higher degree of infiltration levels, while neutrophils showed a higher trend of infiltration levels in the CRLM group (Fig. 2D). The correlation analysis indicated that 9 of 17 monocyte marker genes were related to monocytes, and 3 of 24 neutrophil marker genes were related to neutrophils (Fig. 2E).

Construction and validation of a diagnostic signature

The 9 monocyte marker genes and 3 neutrophil marker genes were assessed by LASSO logistic regression algorithm (Fig. 3A-B). Then, 6 feature genes were selected to construct the diagnostic signature with the following formula: Risk score = (1.662 × SLC11A1) + (1.036 × IFRD1) + (0.462 × IL32) + (-1.373 × KYNU) + (1.344 × TIMP1) + (1.112 × SERPINA1). The AUC values were 0.986 in training set and 0.893 in validation set, suggesting that the predictive ability of the risk score achieved well (Fig. 3C-D). The correlation analysis between risk score and monocyte/neutrophil indicated that risk score was positively correlated with monocyte/neutrophil (Fig. 3E-F). In the CRLM group, 6 feature genes were significant highly expressed in training set, and 4 of 6 feature genes (SLC11A1, IFRD1, TIMP1 and SERPINA1) were significant highly expressed in validation set (Fig. 3G-H). The expression of 6 feature genes in each cell cluster was visualized by bubble plots (Fig. 3I).

Construction of CeRNA network and TF regulatory network

Based on ENCORI database, miRNAs that may target 6 feature genes were predicted. Then, 399 differentially expressed miRNAs were obtained between CRC and CRLM in GSE81581. The miRNAs differentially expressed in GSE56453 and negatively regulated feature genes were intersected, and 12 miRNAs were obtained, corresponding to 4 feature genes. Similarly, the lncRNAs that might regulate these 12 miRNAs were predicted based on ENCORI database. The correlation analysis between predicted lncRNAs and 4 feature genes were performed ($p < 0.05$). Then, 13 predicted lncRNAs that were correlated with 4 feature genes were obtained, corresponding to 8 miRNAs. Ultimately, the ceRNA network, including 13 lncRNAs, 8 miRNAs and 4 mRNAs, was established (Fig. 4A). A total of 58 TFs associated with 6 genes were identified to construct TF regulatory network (Fig. 4B). Among them, SLC11A1 was associated with the most TFs, with 30 TFs, and ADNP and SLC11A1 had the highest correlation (-0.731).

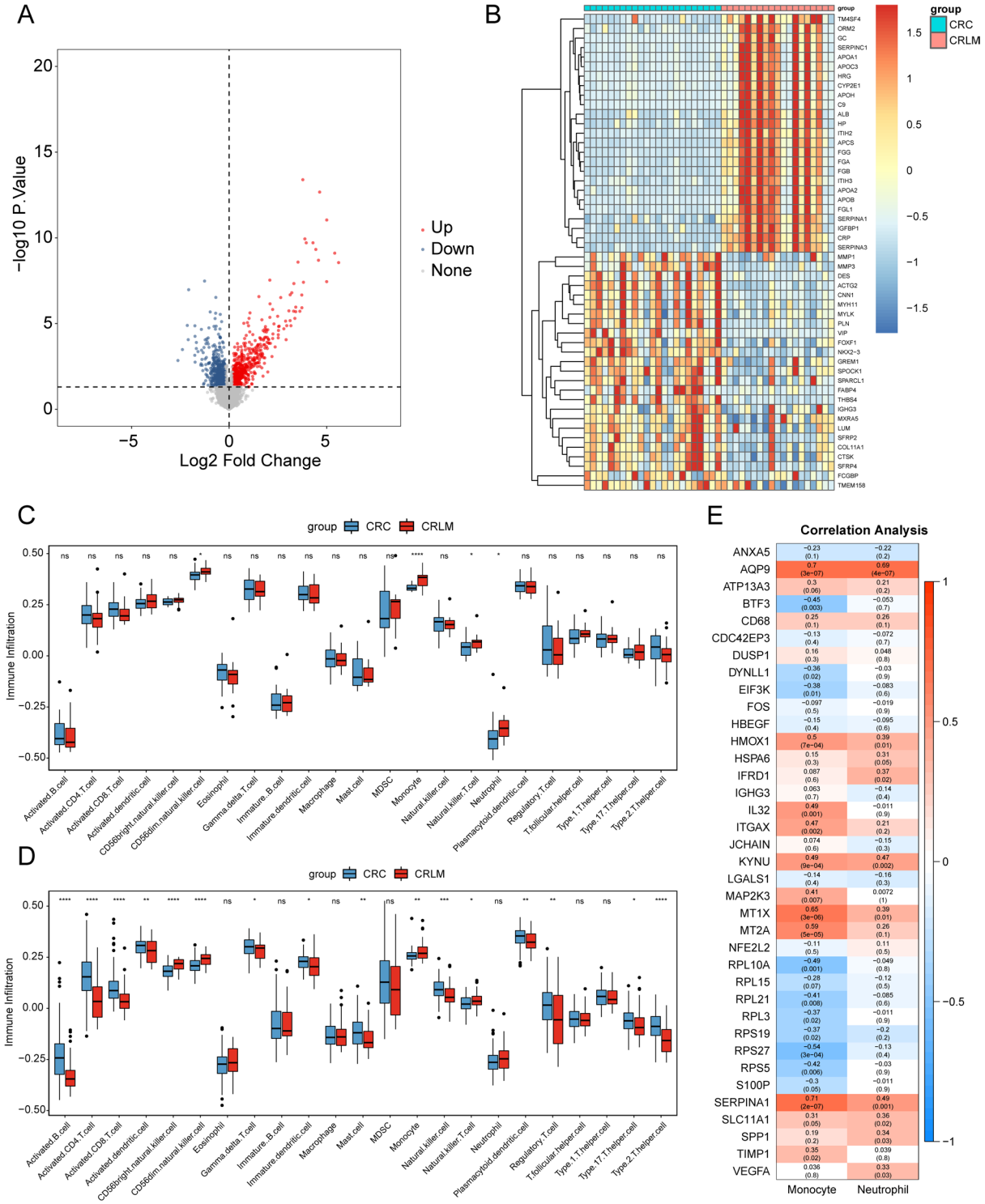

Fig. 2. Differential gene analysis. (**A**) The volcano plot (**A**) and heatmap (**B**) of DEGs between CRC and CRLM in GSE81558. (**C**) The infiltration levels of monocyte and neutrophil in training set. (**D**) The infiltration levels of monocyte and neutrophil in validation set. (**E**) Correlation analysis between monocyte/neutrophil marker genes and monocyte/neutrophil.* indicates a comparison between two groups. * $P<0.05$, ** $P<0.01$, *** $P<0.001$, **** $P<0.0001$, and ns stands for not significant.

RT-qPCR in human subjects and cell lines

The mRNA expression level of SLC11A1 in SLC11A1, IFRD 1, LI32, KYNU, TIMP 1, normal tissues and SERPINA1 were detected by RT-qPCR experiments, and the results showed that the expression difference of SLC11A1 was the most obvious, so we chose SLC11A1 as the main target in subsequent experiments (Fig. 4C).

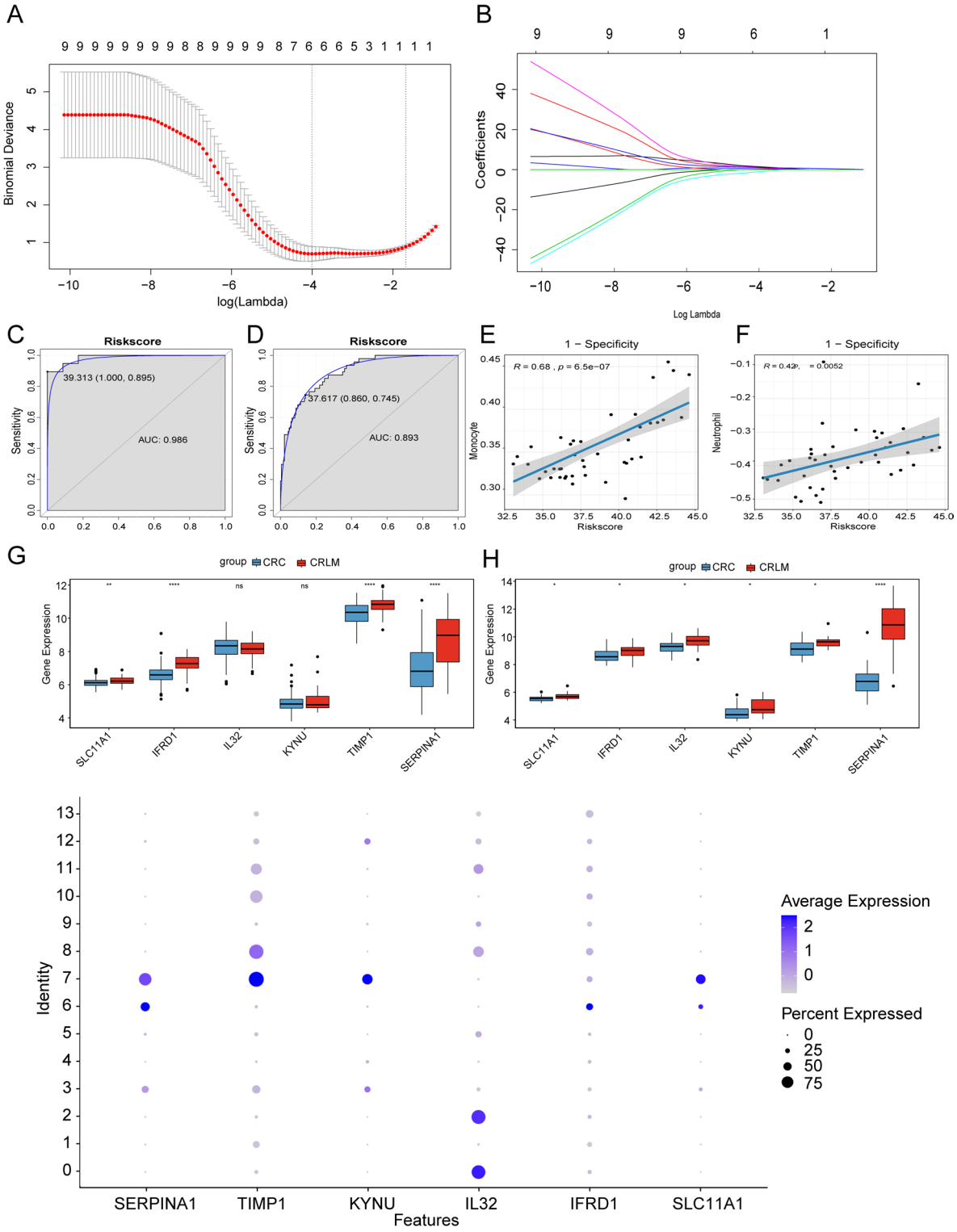

Fig. 3. Construction and validation of a diagnostic signature. (**A**,**B**) The LASSO regression analysis. (**C**,**D**) The AUC of the risk score in training (**C**) and validation (**D**) set. (**E**,**F**) The correlation analysis between risk score and neutrophil (**E**)/monocyte (**F**). (**G**,**H**) The expression level of 6 feature genes in training (**G**) and validation (**H**) set. (**I**) Expression levels of 6 feature genes for each cell cluster. * indicates a comparison between two groups. * $P<0.05$, ** $P<0.01$, **** $P<0.0001$, and ns stands for not significant.

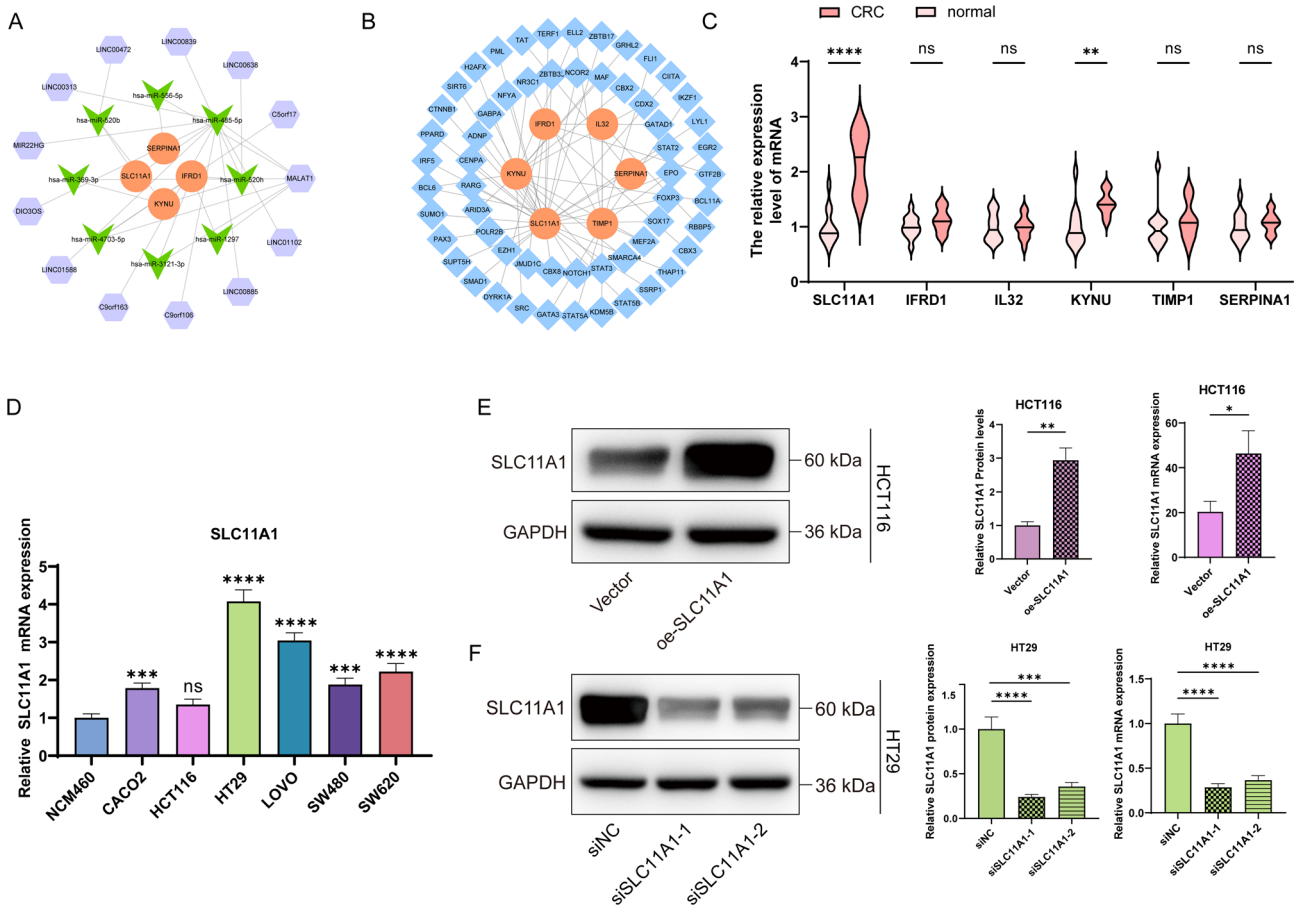

Fig. 4. Differential expression of ceRNA network and SLC11A. (**A**,**B**) The ceRNA network and TF regulatory network. The hexagons, inverted triangles, rhombi, and ellipses indicate lncRNAs, miRNAs, TFs and mRNAs, respectively. Orange and green color represent up- and down-regulation, respectively. (**C**) Detection of the expression levels of SLC11A1, IFRD1, IL32, KYNU, TIMP1 and SERPINA mRNAs in CRC and normal tissues. (**D**) Detection of SLC11A1 mRNA expression levels in NCM460, CACO2, HCT116, HT29, LOVO, SW480, and SW620 cells. (**E**) After transfection with oe-SLC11A1 plasmid for 48 h in HCT116 cells, the expression levels of SLC11A1 protein and mRNA were detected. (**F**) After transfection with siSLC11A1-1 and siSLC11A1-2 interfering RNAs for 48 h in HT29 cells, the expression levels of SLC11A1 protein and mRNA were detected. * indicates a comparison between two groups. * $P<0.05$, ** $P<0.01$, *** $P<0.001$, **** $P<0.0001$, and ns stands for not significant.

We screened for the relative expression levels of SLC11A1 mRNA in different CRC cell lines. The results showed that HT 29 showed the highest mRNA expression and the lowest HCT116, in order to further explore the mechanistic studies of SLC11A1 in CRC (Fig. 4D). We constructed SLC11A1 knockdown cell lines in HT 29 cell line and SLC11A1 overexpression cell lines in HCT116 cell line. Assays by RT-qPCR and Western blot experiments showed successful SLC11A1 knockdown and overexpression cell line construction (Fig. 4E and F).

Knockdown of SLC11A1 was able to inhibit CRC cell proliferation

The results of CCK8 showed that down-regulating SLC11A1 expression in HT29 cell lines could significantly reduce the proliferation capacity of HT29 cells in a time-dependent manner. However, in HCT116 cell line, the proliferation ability of SLC11A1 cells was significantly enhanced after overexpression (Fig. 5A). After that, we further verified the changes of SLC11A1 on the proliferation ability of HT29 and HCT116 cells through EDU experiment, and the results were consistent with CCK8. This suggests that SLC11A1 knockdown can inhibit the proliferation of CRC cells. Knockdown of SLC11A1 was able to inhibit the invasion and migration of CRC cells (Fig. 5B).

Knockdown of SLC11A1 was able to inhibit CRC cell proliferation

The results of scratch experiments showed that down-tapping SLC11A1 expression in HT29 cell lines could significantly reduce the migration ability of HT29 cells in a time-dependent manner. In HCT116 cell line, overexpression of SLC11A1 significantly enhanced cell migration (Fig. 5C). Later, we further verified the changes of SLC11A1's invasion ability on HT29 and HCT116 cells through Transwell experiment. Our results showed that SLC11A1 knockdown inhibited the invasion ability of HT29 cells, while overexpression of SLC11A1

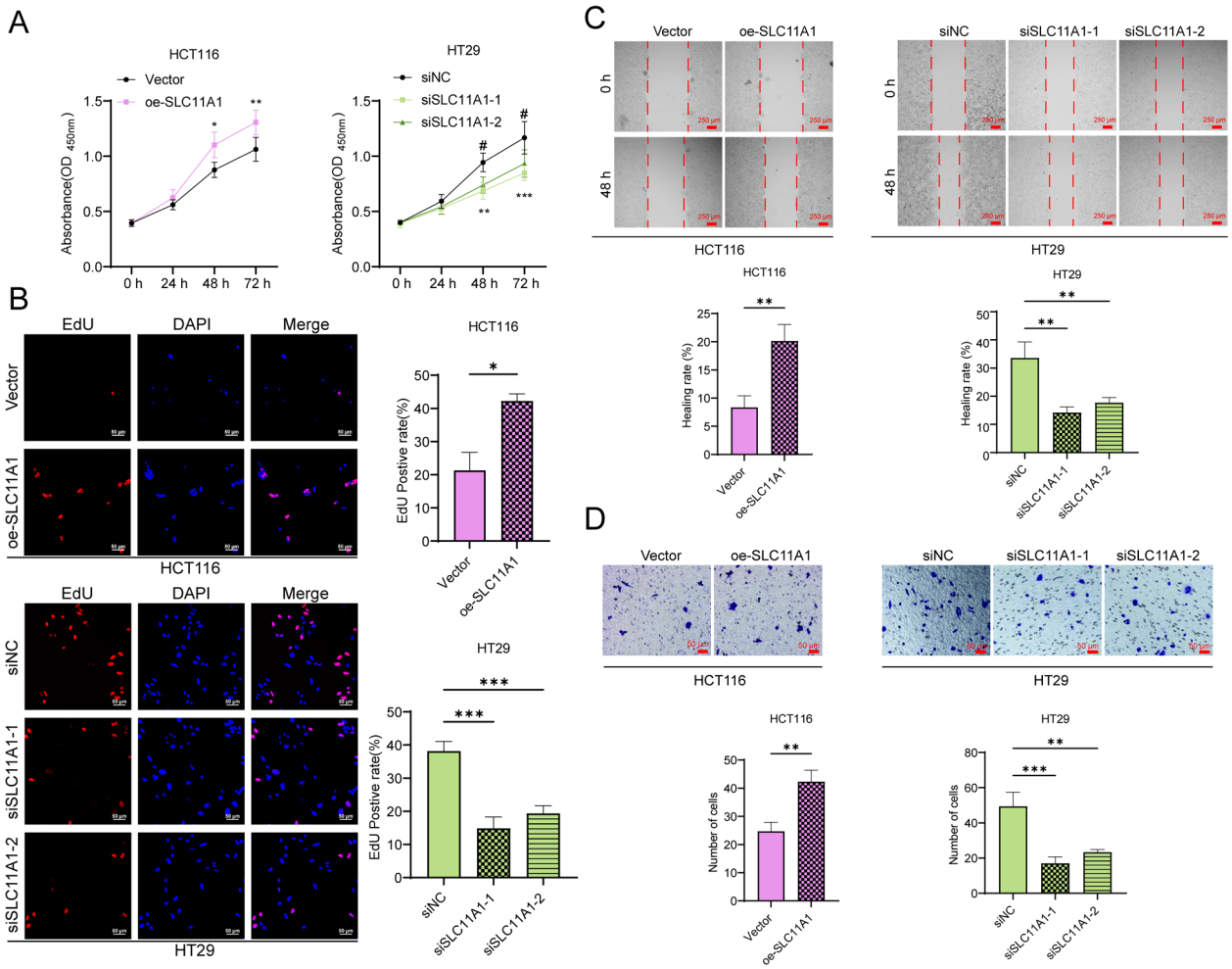

Fig. 5. SLC11A1 induces the proliferation, invasion and migration of CRC cells. (**A**) CCK8 experiments the changes in viability of HT29 and HCT116 cells in different time periods. (**B**) An EDU staining assay was performed for changes in the proliferative capacity of HT29 and HC116 cells. (**C**) Changes in the migratory capacity of HT 29 and HCT116 cells were determined by scratches 48 h after cell transfection. (D)Changes in the invasive capacity of HT 29 and HCT116 cells were determined by Transwell at 48 h after cell transfection. # denotes the comparison between the siSLC11A1-2 group and the siNC group, while * represents the comparison between two groups. * $P<0.05$, ** $P<0.01$, *** $P<0.001$, and # $P<0.05$.

enhanced the invasion ability of HCT116 cells. This suggests that SLC11A1 can induce CRC cell invasion and migration (Fig. 5D).

Knockout of SLC11A1 can induce ferroptosis in CRC cells and inhibit the invasion of CRC cells

After verifying that SLC11A1 was able to induce the proliferation, invasion and migration of CRC cells, we focused on whether it could affect the ferroptosis in CRC cells. We observed the mitochondrial morphology changes in cells after treatment groups by electron microscopy, and we found no significant changes in mitochondrial morphology after SLC11A1 overexpression. However, after SLC11A1 knockdown, mitochondrial morphology is disrupted, as well as outer membrane rupture and reduction or disappearance of mitochondrial cristae (Fig. 6A). And after knockdown of SLC11A1 also led to the accumulation of MDA and Fe^{2+} in HT29 cells (Fig. 6B), upregulated ACSL4, COX2, NOX1 and downregulated GPX4, and the expression level of FIH 1 protein promoted cell ferroptosis (Fig. 7A). In addition, we also detected the expression of invasion - related proteins in HCT116 and HT29 cells. In HCT116 cells, compared with the Vector group, the expression level of E-cadherin in the oe-SLC11A1 group decreased significantly, while the expression levels of N-cadherin and Vimentin increased significantly. In HT29 cells, compared with the si-NC group, the expression level of E-cadherin in the siSCL11A1-1 and siSCL11A1-2 groups increased significantly, while the expression levels of N-cadherin and Vimentin decreased significantly (Fig. 7B). We speculated that the knockdown of SLC11A1 was able to inhibit CRC cell proliferation, and that invasion and migration were most likely achieved through the regulation of ferroptosis.

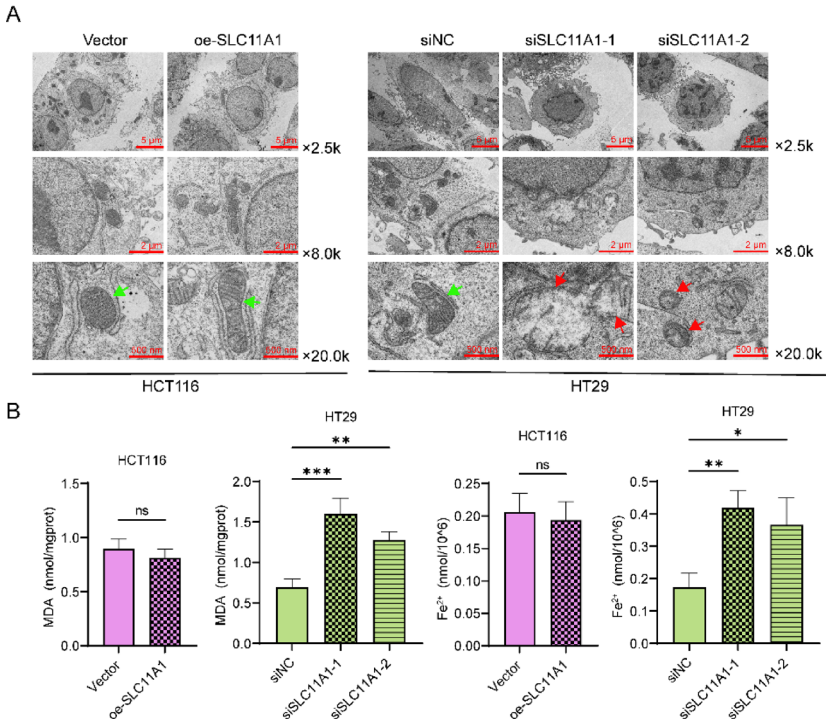

Fig. 6. Knockdown of SLC11A1 induces iron death in CRC cells. (**A**) Electron microscopy to observe the intracellular mitochondrial structure and morphology 48 h after transfection of each group of HT 29 cells and HCT116 cells (The green arrow represents that the mitochondria have a normal morphology, with abundant and dense cristae, almost filling the entire mitochondrial matrix. The outer membrane is smooth, and the outline is clear and continuous. The red arrow represents that the mitochondria are significantly swollen, with reduced, broken cristae, or even a complete disappearance of cristae, and the outer shape shows breaks). (**B**) Changes in intracellular MDA and Fe^{2+} levels were measured 48 h after transfection in each group of HT 29 cells and HCT116 cells. * indicates a comparison between two groups. * $P<0.05$, ** $P<0.01$, *** $P<0.001$, and ns stands for not significant.

SLC11A1 is able to activate the TGFβ1 signaling pathway

To confirm that SLC11A1 can target the TGFβ1 signaling pathway, we detected the presence of TGFβ1 protein in the SCL11A1 protein complex through the Co-IP assay. The results showed that both TGFβ1 and SCL11A1 proteins were present in the protein complexes pulled down by SCL11A1 in HCT116 and HT29 cells. These findings confirm the interaction between SCL11A1 and TGFβ1, providing evidence that SLC11A1 can target the TGFβ1 signaling pathway (Fig. 8A).

We examined key proteins in the TGFβ1 signaling pathway by a Western blot assay. The results showed that SLC11A1 overexpression was able to activate the protein expression levels of p-Smad 2 / 3 and TGFβ1, with no obvious effect on the Smad 2 / 3 proteins. The protein expression levels of p-Smad 2 / 3 and TGFβ1 were repressed upon knockdown of SLC11A1 in HCT116 cells. This also suggests that SLC11A1 is able to activate the TGFβ1 signaling pathway (Fig. 8B).

To further provide evidence that SLC11A1 targets the TGFβ1 signaling pathway, we designed a reverse - validation experiment by introducing LSKL (an inhibitor of the TGFβ1 signaling pathway) and 10 ng/mL TGFβ1 (an activator of the TGFβ1 signaling pathway). The experimental results showed that, in HCT116 cells, compared with the oe-SLC11A1 group, the ratio of p-Smad2/3 to Smad2/3 and the expression level of TGFβ1 decreased in the oe-SLC11A1 + LSKL group. In HT29 cells, compared with the si-SLC11A1-1 group, the ratio of p-Smad2/3 to Smad2/3 and the expression level of TGFβ1 increased in the si-SLC11A1-1 + TGFβ1 (10 ng/mL) group (Fig. 8C).

Discussion

We finally chose SLC11A1 for study based on online database and subsequent validation of CRC tissue and cell samples. SLC11A1 belongs to the solute carrier family 11 family, a proinflammatory factor located in monocytes that is closely correlated with susceptibility to autoimmune and infectious diseases[18]. Moreover, SLC11A1 is associated with various cancers. Polymorphisms of SLC11A1 were implicated in bladder cancer recurrence[19]. Zhu et al. indicated that SLC11A1 was related to the increased risk and poor prognosis in prostate cancer[20]. SLC11A1 was identified to serve as a prognostic marker and immunotherapy response indicator in glioma[21]. Ma et al. suggested that SLC11A1 could serve as a significant indicator for predicting poor prognosis and immunotherapy efficacy in CRC[22]. Despite this, there is no studies to explore the function of SLC11A1 in CRLM progression, and the potential molecular mechanism is poorly understood. In our study, we found that

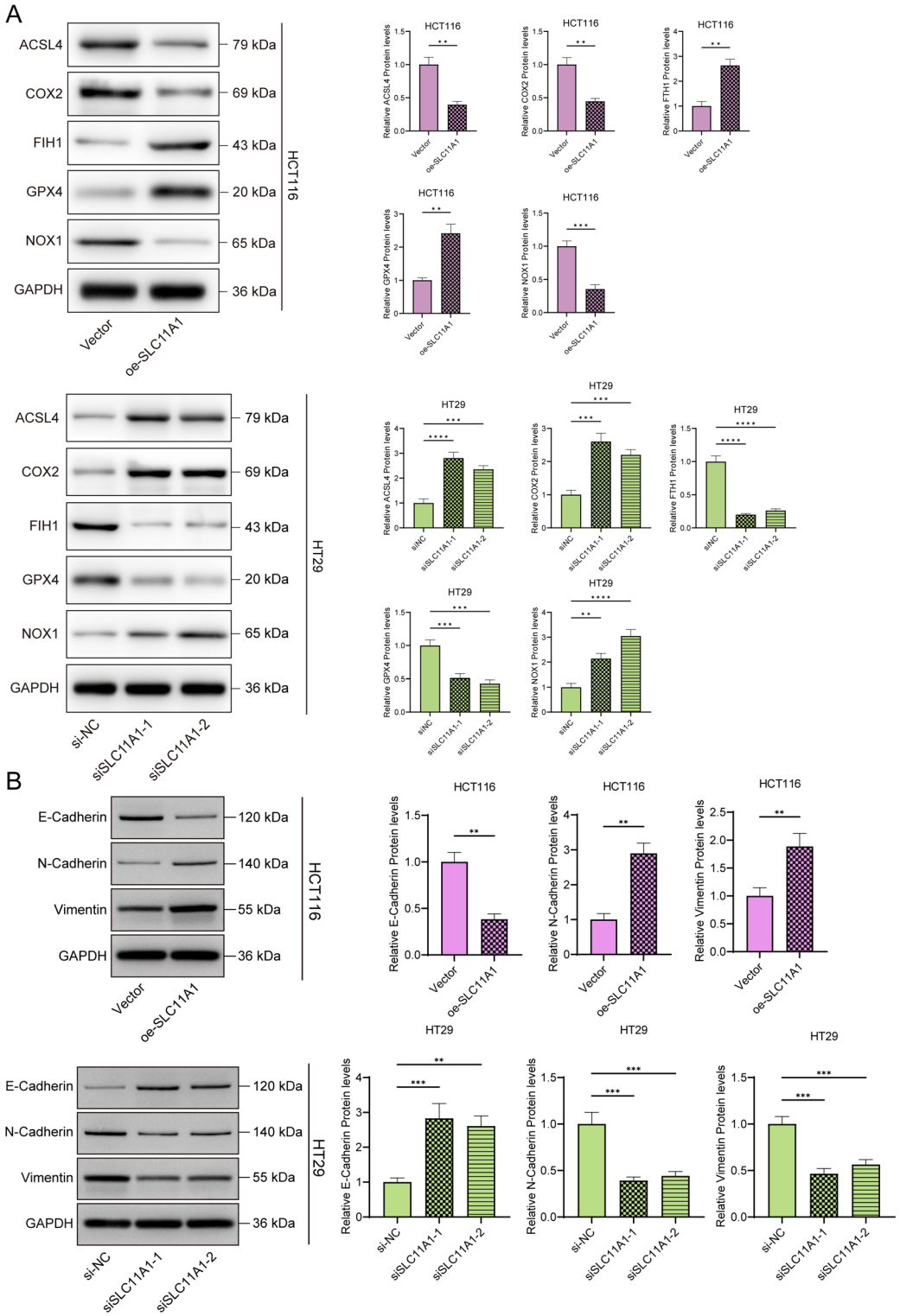

Fig. 7. SCL11A1 can regulate ferroptosis - and EMT - related marker proteins. (**A**) After 48 h of transfection with overexpression plasmids and small interfering RNAs in HCT116 and HT29 cells, the relative expression levels of ACSL4, COX2, FIH1, GPX4, and NOX1 proteins were detected by Western blot assay. (**B**) The expression levels of E - cadherin, N - cadherin and Vimentin proteins in HCT116 and HT29 cells (which had undergone cell transfection according to the requirements of each group) were detected by Western blot assay. * indicates a comparison between two groups. ** $P < 0.01$, *** $P < 0.001$, **** $P < 0.0001$.

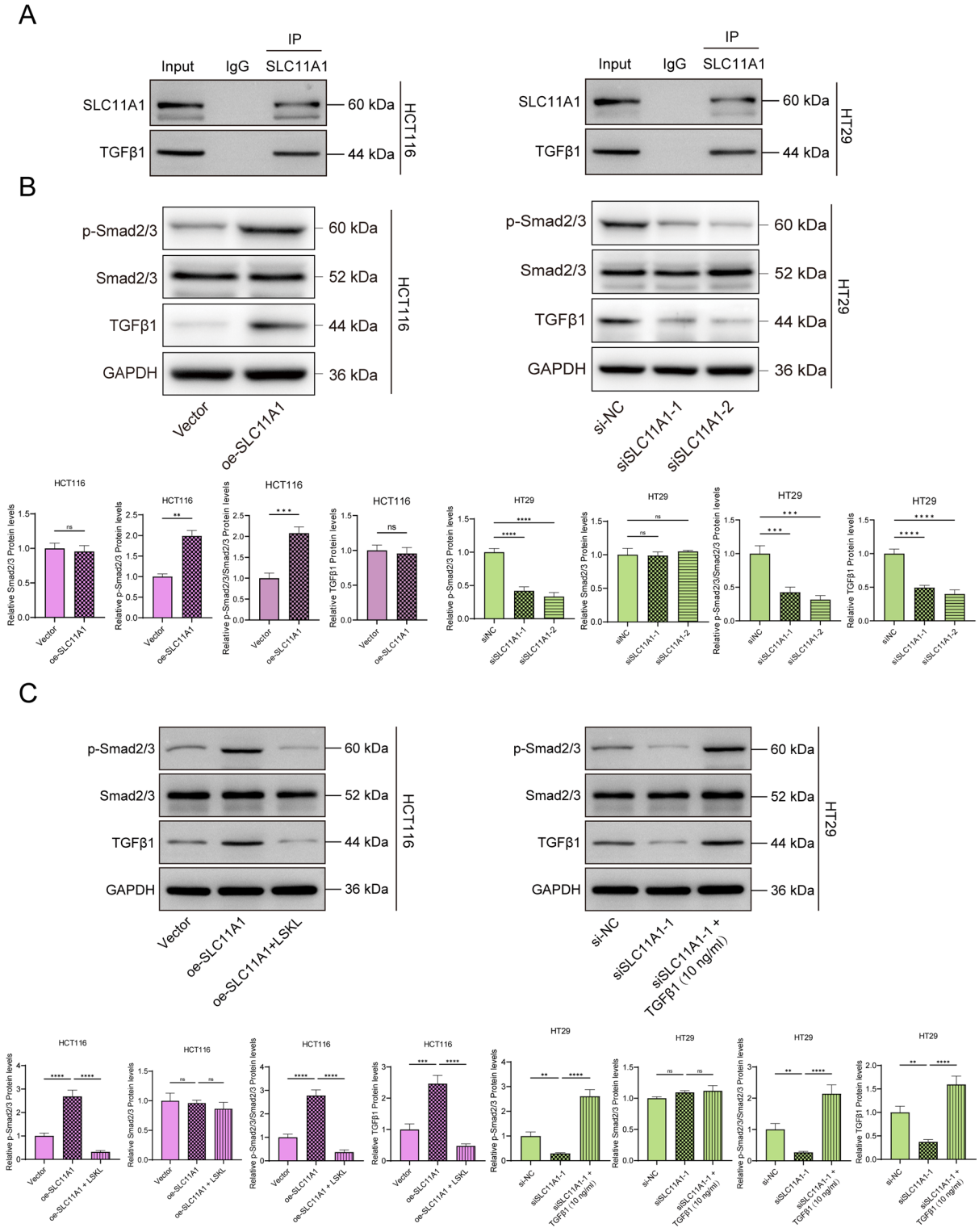

Fig. 8. SLC11A1 Activate the TGFβ1 signaling pathway. (**A**) In HCT116 and HT29 cells, co - immunoprecipitation was used to detect the expression of SCL11A1 and TGFβ1 in the protein complex pulled down by SLC11A1. (**B**) After 48 h of transfection with overexpression plasmids and small interfering RNAs in HCT116 and HT29 cells, the relative expression levels of Smad 2/3, p-Smad 2/3, and TGFβ1 proteins were detected by Western blot assay. (**C**) In HCT116 cells, after transfecting the over-expression plasmid for 48 h, LSKL (an inhibitor of the TGF-β1 pathway) was added and the cells were incubated for an additional 24 h. In HT29 cells, after transfecting siRNA for 48 h, 10 ng/mL TGF-β1 (an activator of the TGF - β1 pathway) was added. After these treatments for both types of cells, the protein expression levels of Smad 2/3, p-Smad 2/3, and TGF-β1 were detected by Western blot assay. * indicates a comparison between two groups. ** $P < 0.01$, *** $P < 0.001$, **** $P < 0.0001$.

SLC11A1 was highly expressed in both CRC tissues and cells, and after our SLC11A1 knockdown, CRC cell proliferation was significantly decreased, and invasion and migration were also significantly decreased. During the process of tumor invasion, the expression changes of E-cadherin, N-cadherin, and Vimentin are closely related and jointly regulate the epithelial-mesenchymal transition (EMT) process. As an epithelial marker, the down - regulation of E-cadherin expression weakens intercellular adhesion, thereby facilitating the detachment of tumor cells from the primary tumor site[23,24]. On the other hand, as mesenchymal markers, the up-regulation of N-cadherin and Vimentin expressions enhances the migration and invasion capabilities of cells[25]. This shift in molecular phenotype not only endows cells with greater motility but also helps them break through the basement membrane and invade surrounding tissues, ultimately promoting tumor metastasis[26]. The results of this study show that after overexpressing SLC11A1, the expression level of E-cadherin decreased significantly, while the expression levels of N-cadherin and vimentin increased significantly. This is consistent with the previous studies.

It has been reported that SLC11A1 is closely related to cellular iron homeostasis, and iron death occurs when the iron ion balance in the cell is broken, such as iron overload or iron deficiency[27,28]. Some studies have found that there is iron overload and lipid peroxidation in CRC cells, which may be related to the occurrence and development of CRC[29,30]. However, the mechanism by which SLC11A1 mediates iron death in CRC has not been reported. Our study found that knocking down the expression of SLC11A1 increased the accumulation of MDA and Fe^{2+} in CRC cells, leading to mitochondrial structure damage and inducing cell iron death. GPX4 is one of the major intracellular antioxidant enzymes, and the reduced activity of GPX4 leads to increased intracellular lipid peroxidation[31]. While the expression of ACSL4 was increased, leading to increased intracellular lipid peroxidation[32]. ROS is believed to play a key role in the process of lipid peroxidation[33]. NOX1 is an important ROS (reactive oxygen species) -generating enzyme, which can transfer electrons from NADPH to oxygen molecules and produce ROS such as superoxide anions[34,35]. COX2 and HIF1 are also thought to be closely related to ROS[36,37]. Our study showed that SLC11A1 knockdown was able to downregulate FIH1 and GPX4 and upregulate the expression levels of ACSL4, COX2, and NOX1, inducing cells to undergo iron death, which further strengthened the evidence that SLC11A1 is able to regulate iron death. We then explored the possible mechanisms of SLC11A1 regulation, focusing on the TGFβ1 signaling pathway. It has been reported that high expression of SLC11A1 in colorectal cancer is significantly enriched in TGFβ1 pathway, JAK-STAT pathway and angiogenesis[22]. Abnormal activation of TGFβ1 signaling pathway can promote CRC cell invasion, metastasis and EMT process, and enhance CRC cell proliferation[38]. Therefore, inhibition of TGFβ1 signaling pathway helps to inhibit the progression of CRC. In addition, the ability of TGFβ1 signaling to regulate the ferroptosis process has been confirmed by numerous studies[39]. The COIP experiment also confirmed the interaction between SLC11A1 and TGFβ1. In the reverse validation experiment, the addition of LSKL could reverse the activation of the TGFβ1 signaling pathway caused by the overexpression of SLC11A1. Conversely, the addition of TGFβ1 (10 ng/mL) could reverse the inhibitory effect on the signaling pathway caused by the knockdown of SLC11A1. This provides strong evidence that SLC11A1 targets the TGFβ1 signaling pathway.

The biggest innovation of this study lies in the revelation that SLC11A1 can promote CRC cell proliferation, invasion and migration resistance to CRC cell ferroptosis, and the possible mechanism is achieved through the activation of TGFβ1 signaling pathway. Although our results are encouraging, there are still some limitations. First of all, the conclusions of this study were only verified at the in - vitro experimental level, lacking evidence from in - vivo experiments. In the future, we will prioritize the establishment of "humanized mouse xenograft and metastasis models with conditional knockout and overexpression of SLC11A1" in our subsequent research. Although the changes in the expression of ACSL4 and GPX4 suggest that ferroptosis may be involved, we have not completely ruled out the potential effects of other forms of cell death, such as apoptosis, pyroptosis, and cuproptosis. In subsequent studies, we will systematically evaluate the key markers of various types of cell death to clarify whether SLC11A1 specifically regulates ferroptosis or exerts its effects by coordinating multiple cell death pathways.

Conclusion

We found that SLC11A1 is aberrantly expressed in CRC. Knockdown of SLC11A1 inhibited TGFβ1 signaling, suppressed CRC cell progression, and promoted MDA and Fe2 + accumulation, thereby inducing ferroptosis. SLC11A1 may promote resistance to ferroptosis, partially through TGF-β1 signaling, though other mechanisms (e.g., ROS regulation) may also contribute. These results suggest that SLC11A1 can be used as a clinical drug target and provide a theoretical basis for subsequent drug development.

Data availability

The data regarding the results of this study can be requested from the corresponding author upon reasonable request.

Received: 3 March 2025; Accepted: 15 December 2025
Published online: 23 December 2025

References

1. Sung, H. et al. Global cancer statistics 2020: Globocan estimates of incidence and mortality worldwide for 36 cancers in 185 countries. *Ca Cancer J. Clin.* **71**, 209–249 (2021).
2. Biller, L. H. & Schrag, D. Diagnosis and treatment of metastatic colorectal cancer: A review. *Jama* **325**, 669–685 (2021).
3. Poturnajova, M. et al. Molecular features and gene expression signature of metastatic colorectal cancer (review). *Oncol. Rep.* **45** (2021).
4. Shin, A. E., Giancotti, F. G. & Rustgi, A. K. Metastatic colorectal cancer: mechanisms and emerging therapeutics. *Trends Pharmacol. Sci.* **44**, 222–236 (2023).

5. Zygulska, A. L. & Pierzchalski, P. Novel diagnostic biomarkers in colorectal cancer. *Int J. Mol. Sci.* **23** (2022).
6. Dekker, E., Tanis, P. J., Vleugels, J., Kasi, P. M. & Wallace, M. B. Colorectal cancer. *Lancet* **394**, 1467–1480 (2019).
7. Tzavlaki, K. & Moustakas, A. Tgf-Beta signaling. *Biomolecules*. **10** (2020).
8. Derynck, R., Turley, S. J. & Akhurst, R. J. Tgfbeta biology in cancer progression and immunotherapy. *Nat. Rev. Clin. Oncol.* **18**, 9–34 (2021).
9. Ali, S. et al. Tgf-Beta signaling pathway: therapeutic targeting and potential for anti-cancer immunity. *Eur. J. Pharmacol.* **947**, 175678 (2023).
10. Gough, N. R., Xiang, X. & Mishra, L. Tgf-Beta signaling in liver, pancreas, and gastrointestinal diseases and cancer. *Gastroenterology* **161**, 434–452 (2021).
11. Tang, Q. et al. Tm4Sf1 promotes Emt and cancer stemness via the Wnt/Beta-Catenin/Sox2 pathway in colorectal cancer. *J. Exp. Clin. Cancer Res.* **39**, 232 (2020).
12. Liu, A. et al. Prmt5 methylating Smad4 activates Tgf-Beta signaling and promotes colorectal cancer metastasis. *Oncogene* **42**, 1572–1584 (2023).
13. Shasha, T., Gruijs, M. & van Egmond, M. Mechanisms of colorectal liver metastasis development. *Cell. Mol. Life Sci.* **79**, 607 (2022).
14. Gao, Y., Li, H., Wang, P., Wang, J. & Yao, X. Sik1 suppresses colorectal cancer metastasis and chemoresistance via the Tgf-Beta signaling pathway. *J. Cancer*. **14**, 2455–2467 (2023).
15. Bong, D., Sohn, J. & Lee, S. V. Brief guide to Rt-Qpcr. *Mol. Cells*. **47**, 100141 (2024).
16. Song, S. et al. Sestrin2 remedies podocyte injury via orchestrating Tsp-1/Tgf-Beta1/Smad3 axis in diabetic kidney disease. *Cell. Death Dis.* **13**, 663 (2022).
17. Ge, A. et al. Diosmetin prevents Tgf-Beta1-induced epithelial-mesenchymal transition via Ros/Mapk signaling pathways. *Life Sci.* **153**, 1–8 (2016).
18. Archer, N. S., Nassif, N. T. & O'Brien, B. A. Genetic variants of Slc11a1 are associated with both autoimmune and infectious diseases: systematic review and meta-analysis. *Genes Immun.* **16**, 275–283 (2015).
19. Decobert, M. et al. Polymorphisms of the human Nramp1 gene are associated with response to Bacillus Calmette-Guerin immunotherapy for superficial bladder cancer. *J. Urol.* **175**, 1506–1511 (2006).
20. Zhu, Q. et al. Association of genetic variants in autophagy-lysosome pathway genes with susceptibility and survival to prostate cancer. *Gene* **808**, 145953 (2022).
21. Xu, H. et al. Slc11a1 as a stratification indicator for immunotherapy or chemotherapy in patients with glioma. *Front. Immunol.* **13**, 980378 (2022).
22. Ma, Y., Zhan, L., Yang, J. & Zhang, J. Slc11a1 associated with tumor microenvironment is a potential biomarker of prognosis and immunotherapy efficacy for colorectal cancer. *Front. Pharmacol.* **13**, 984555 (2022).
23. Rubtsova, S. N., Zhitnyak, I. Y. & Gloushankova, N. A. Dual role of E-Cadherin in cancer cells. *Tissue Barriers*. **10**, 2005420 (2022).
24. van Loon, K., van Breest, S. M., Huijbers, E., Griffioen, A. W. & van Beijnum, J. R. Extracellular vimentin as a versatile immune suppressive protein in cancer. *Biochim. Biophys. Acta-Rev Cancer*. **1878**, 188985 (2023).
25. Gouin, K. R. et al. An N-Cadherin 2 expressing epithelial cell subpopulation predicts response to Surgery, chemotherapy and immunotherapy in bladder cancer. *Nat. Commun.* **12**, 4906 (2021).
26. Luond, F. et al. Distinct contributions of partial and full Emt to breast cancer malignancy. *Dev. Cell.* **56**, 3203–3221 (2021).
27. Dighal, A. et al. Iron trafficking in patients with Indian post Kala-Azar dermal leishmaniasis. *Plos Negl. Trop. Dis.* **14**, e7991 (2020).
28. Gomez, M. A. et al. Protein tyrosine phosphatases are regulated by mononuclear iron dicitrate. *J. Biol. Chem.* **285**, 24620–24628 (2010).
29. Liu, X. et al. Ferroptosis: reviewing crc with the third eye. *J. Inflamm. Res.* **15**, 6801–6812 (2022).
30. Yan, H., Talty, R. & Johnson, C. H. Targeting ferroptosis to treat colorectal cancer. *Trends Cell. Biol.* **33**, 185–188 (2023).
31. Xue, Q. et al. Copper-dependent autophagic degradation of Gpx4 drives ferroptosis. *Autophagy* **19**, 1982–1996 (2023).
32. Wang, Y. et al. Acsl4 deficiency confers protection against ferroptosis-mediated acute kidney injury. *Redox Biol.* **51**, 102262 (2022).
33. Zorov, D. B., Juhaszova, M. & Sollott, S. J. Mitochondrial reactive oxygen species (Ros) and Ros-induced Ros release. *Physiol. Rev.* **94**, 909–950 (2014).
34. Hsu, N. Y. et al. Nox1 is essential for Tnfalpha-Induced intestinal epithelial Ros secretion and inhibits M cell signatures. *Gut* **72**, 654–662 (2023).
35. Makhezer, N. et al. Nox1-Derived Ros drive the expression of Lipocalin-2 in colonic epithelial cells in inflammatory conditions. *Mucosal Immunol.* **12**, 117–131 (2019).
36. Hou, F. Q. et al. Trilobatin rescues fulminant hepatic failure by targeting Cox2: involvement of Ros/Tlr4/Nlrp3 signaling. *Phytomedicine* **120**, 155059 (2023).
37. Li, L., Tan, J., Miao, Y., Lei, P. & Zhang, Q. Ros and autophagy: interactions and molecular regulatory mechanisms. *Cell. Mol. Neurobiol.* **35**, 615–621 (2015).
38. Bao, W., Wang, J., Fan, K., Gao, Y. & Chen, J. Pias3 promotes ferroptosis by regulating Txnip via Tgf-Beta signaling pathway in hepatocellular carcinoma. *Pharmacol. Res.* **196**, 106915 (2023).
39. Yang, Z. et al. Calcipotriol suppresses Gpx4-mediated ferroptosis in Oa chondrocytes by blocking the Tgf-Beta1 pathway. *Cytokine* **171**, 156382 (2023).

Author contributions

D.Q.Y., L.M.Z. and P.S. conceived, designed, and supervised the study. J.F.Z., G.Y. and B.S. performed data analysis and drafed the manuscript. G.I.W. and J.C.X.collected the data, H.Q.M. and B.K.L. arranged the fgures. X.H.H., F.F.W. and G.Y.W. revised the manuscript. All authors reviewed and approved the fnal manuscript.

Funding

National Natural Science Foundation of China (82272909); Hebei Province Natural Innovation Group project (H2022206355); Hebei Province Major Science and Technology Support Program (242W7711Z).

Declarations

Consent to participate

All studies involving humans obtained written informed consent from participants.

Ethics approval

All studies involving humans were approved by the Medical Ethics Committee of Fourth Hospital of Hebei Medical University in August 2020 (2020KV102).

Competing interests
The authors declare no competing interests.

Additional information
Supplementary Information The online version contains supplementary material available at https://doi.org/10.1038/s41598-025-32979-8.

Correspondence and requests for materials should be addressed to G.W.

Reprints and permissions information is available at www.nature.com/reprints.

Publisher's note Springer Nature remains neutral with regard to jurisdictional claims in published maps and institutional affiliations.